15th World Congress on Computational Mechanics (WCCM-XV)
8th Asian Pacific Congress on Computational Mechanics (APCOM-VIII)
Virtual Congress: 31 July – 5 August 2022
S. Koshizuka (Ed.)

FULL-WAVEFORM INVERSION OF SEISMIC INPUT MOTIONS AT A DOMAIN REDUCTION METHOD BOUNDARY IN A PML-TRUNCATED DOMAIN

BRUNO GUIDIO[1], HEEDONG GOH[2], CHANSEOK JEONG[1]

[1] School of Engineering and Technology, Central Michigan University,
Mount Pleasant, MI 48859, USA
[2] Department of Electrical and Computer Engineering, The University of Texas at Austin,
Texas, TX 78712, USA
peruq1b@cmich.edu (the presenting author) & jeong1c@cmich.edu (the corresponding author)

Key words: Passive-seismic inversion, Domain reduction method (DRM), Non-convolutional CFS-PML, Full-waveform inversion (FWI)

Abstract. *A new inverse modeling is investigated for identifying an effective seismic force at virtual interfaces and estimating the seismic wave motions in an interior domain surrounded by a domain reduction method (DRM) boundary from limited seismic measurement data. The two-dimensional domain is truncated by the highly efficient non-convolutional second-order complex-frequency-shifted perfectly matched layers (CFS-PML), and the DRM is utilized to model seismic input motions coming from the outside domain of the CFS-PML. A partial differential equation (PDE)-constrained optimization method aims at minimizing a misfit between measured ground motions at sparsely-distributed sensors on the surface induced by surface wave-dominant incident waves (or equivalent effective forces on a DRM layer) and their estimated counterparts induced by inverted effective forces. The numerical results show that the presented full-waveform inversion of seismic input motions can identify an effective seismic force at a DRM layer and reconstruct the seismic wave responses in a near-surface domain.*

1 INTRODUCTION

There is a need for estimating incident seismic wavefields in a soil-structure system from sparse seismic measurement data. Existing methods are limited to large-scale seismic-source inversion approaches [1] and deconvolution [14, 16, 18, 19]. This paper presents an alternative method for reconstructing incoherent seismic input motions in a near-surface truncated domain. The presented method would have lower computational cost and more accurate geophysical data than large-scale source inversion, and it would not be limited to a 1D setting as opposed to deconvolution. Such a potential method can allow engineers to pinpoint where large amplitudes of stress waves occur (or structural failures occur) in built environments in a domain of interest during seismic events. It also would help decision-makers quickly plan the budget and schedule repairs after an earthquake event. To this end, incoming seismic motions that shake a domain should be characterized. There have been studies in the geotechnical site characterization, reporting the possibility of utilizing sparsely measured wave motion data for a PDE-constrained optimization [2–4, 6, 7, 12, 15, 17, 20]. Such utilization of measured ground motions is a robust technique that could be employed in the full-waveform inversion of seismic input motions.

In this presented research, a new partial differential equation (PDE)-constrained optimization method to identify incident wave motions (or equivalent forces) from seismic measurement data is proposed as

a potential method to estimate incident seismic wavefields. Toward developing such a potential method, the authors have investigated a novel inverse-source modeling method in a 1D semi-infinite domain [13], a 2D bounded domain of anti-plane motion [11], and a 2D unbounded domain of anti-plane motion truncated by an absorbing boundary condition [10] and that endowed by a DRM boundary [9]. It has been shown that the authors' method has been effective in those scalar-wave settings. Continuing these previous studies, the authors extend the approach to an elastodynamic wave setting. In addition to continuing to use the DRM, this work truncates a 2D plane-strain domain by using the non-convolutional second-order CFS-PML. Namely, in the authors' previous study [10], the reconstructed DRM force, before the postprocessing, creates the outgoing waves of a large amplitude outside the DRM layer. Thus, employing a robust ABC is necessary to prevent the outgoing waves from being reflected from the truncated boundary. Then in the presented work, the non-convolutional second-order CFS-PML [8], a more robust absorbing boundary, is implemented. Finally, this paper investigate the presented full-waveform inversion method for (*i*) identifying an effective seismic force at a DRM layer from ground motions on the surface and (*ii*) consequently reconstructing the wave responses in an interior domain.

2 GOVERNING WAVE PHYSICS

Fig. 1 displays the problem configuration where incident waves are propagated in an enlarged 2D undamped domain truncated by CFS-PML and generate synthetic data for the presented study. Moreover, Fig. 1 shows the heterogeneous domain with its wave speeds V_{s_1}, V_{s_2}, and V_{s_3}, and inclusions with their wave speeds V_{s_4}, V_{s_5}, and V_{s_6}.

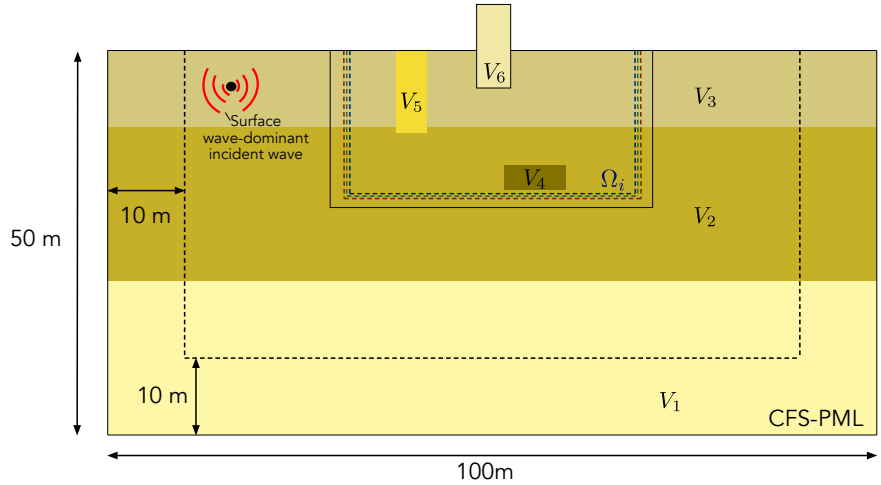

Figure 1: Problem configuration.

The governing equation for the 2D plane-strain setting where elastic waves (comprising P, S, and surface waves) propagate in x and y directions, and their particle movements are in x and y direction, is:

$$\nabla \cdot \boldsymbol{\sigma} - \rho \ddot{\mathbf{u}} = \mathbf{f}, \tag{1}$$

where $\mathbf{u} = [u_x, u_y]^T$ denotes the displacement field, $\ddot{\mathbf{u}}$ denotes the acceleration field, ρ is the mass density, and $\boldsymbol{\sigma}$ represents the stress tensor. The constitutive law in linear, elastic, and isotropic material, which is the stress-strain relation, is defined as:

$$\sigma = \mathbf{C}\varepsilon, \tag{2}$$

where $\mathbf{C}$ is the elasticity tensor, which in the plane-strain setting is written as:

$$\mathbf{C} = \frac{E}{(1+\nu)(1-2\nu)} \begin{bmatrix} 1-\nu & \nu & 0 \\ \nu & 1-\nu & 0 \\ 0 & 0 & \frac{(1-2\nu)}{2} \end{bmatrix} \tag{3}$$

where E and ν are the Young's modulus and the Poisson's ratio of the medium, respectively. The strain tensor ε is defined as:

$$\varepsilon = \mathbf{D}\mathbf{u}, \tag{4}$$

where $\mathbf{D}$ represents the differential operator matrix:

$$\mathbf{D} = \begin{bmatrix} \frac{\partial}{\partial x} & 0 \\ 0 & \frac{\partial}{\partial y} \\ \frac{\partial}{\partial y} & \frac{\partial}{\partial x} \end{bmatrix}. \tag{5}$$

We assume that the external force $\mathbf{f}$ is localized far from the domain of interest (i.e., the DRM-reduced domain Ω_i). Thus, the force term is non-zero only for generating synthetic seismic data in an enlarged domain (see Fig. 1). In all other computations, the far-field seismic source is replaced by a virtual force using the DRM [5, 21].

The top surface of the medium is subject to traction-free conditions:

$$\sigma\mathbf{n} = 0, \quad \text{on } \Gamma_{\text{top}}, \tag{6}$$

where $\mathbf{n}$ is the outward unit normal vector. The left, bottom, and right exterior PML boundaries are constrained by fixed boundary conditions:

$$\mathbf{u} = 0, \quad \text{on } \Gamma_{\text{left}}, \Gamma_{\text{bottom}}, \Gamma_{\text{right}}. \tag{7}$$

The semi-infinite extent of the enlarged domain is truncated by the non-convolutional second-order CFS-PML [8], and we also truncate the domain of interest (i.e., the DRM-reduced domain) by using the CFS-PML. As the semi-infinite physical domain is initially at rest, the initial conditions are:

$$\begin{aligned} \mathbf{u}(x,y,0) &= 0, \\ \dot{\mathbf{u}}(x,y,0) &= 0. \end{aligned} \tag{8}$$

3 NUMERICAL MODELING

The finite element method is used to obtain the numerical solutions of governing equation (1), where its semi-discrete equation reads:

$$\mathbf{M}\ddot{\mathbf{d}}(t) + \mathbf{C}\dot{\mathbf{d}}(t) + \mathbf{K}\mathbf{d}(t) = \mathbf{F}(t). \tag{9}$$

In the above, $\mathbf{d}$ is the solution vector, and $\dot{\mathbf{d}}$ and $\ddot{\mathbf{d}}$ are its first and second time derivative, respectively. Then, we solve the time-dependent equation (9), by considering the initial-value conditions (8) and applying the implicit Newmark time integration, in the following compact form:

$$\mathbf{Q}\hat{\mathbf{d}} = \hat{\mathbf{F}}, \tag{10}$$

where the matrix $\mathbf{Q}$ is the discrete forward operator, which is comprised of the $\mathbf{M}$, $\mathbf{C}$, and $\mathbf{K}$ matrices and defined per the Newmark time integration; and the vectors $\hat{\mathbf{d}}$ and $\hat{\mathbf{F}}$ represent the solution vector and global force vector, respectively, for all the time steps. These vectors are built as:

$$\hat{\mathbf{d}} = \begin{bmatrix} \mathbf{d}_0 \\ \dot{\mathbf{d}}_0 \\ \ddot{\mathbf{d}}_0 \\ \vdots \\ \mathbf{d}_\mathrm{N} \\ \dot{\mathbf{d}}_\mathrm{N} \\ \ddot{\mathbf{d}}_\mathrm{N} \end{bmatrix}, \quad \hat{\mathbf{F}} = \begin{bmatrix} 0 \\ 0 \\ \mathbf{F}_0 \\ \vdots \\ \mathbf{F}_\mathrm{N} \\ 0 \\ 0 \end{bmatrix}, \tag{11}$$

where N is the number of time steps, and $\mathbf{u}_j$ are the spatial degrees of freedom at the j-th time step. Finally, the matrix $\mathbf{Q}$ is defined as:

$$\mathbf{Q} = \begin{bmatrix} \mathbf{I} & 0 & 0 & 0 & 0 & 0 & \dots & 0 & 0 & 0 & 0 & 0 & 0 \\ 0 & \mathbf{I} & 0 & 0 & 0 & 0 & \dots & 0 & 0 & 0 & 0 & 0 & 0 \\ \mathbf{K} & \mathbf{C} & \mathbf{M} & 0 & 0 & 0 & \dots & 0 & 0 & 0 & 0 & 0 & 0 \\ \mathbf{L}_1 & \mathbf{L}_2 & \mathbf{L}_3 & \mathbf{Keff} & 0 & 0 & \dots & 0 & 0 & 0 & 0 & 0 & 0 \\ a_1\mathbf{I} & \mathbf{I} & 0 & -a_1\mathbf{I} & \mathbf{I} & 0 & \dots & 0 & 0 & 0 & 0 & 0 & 0 \\ a_0\mathbf{I} & a_2\mathbf{I} & \mathbf{I} & -a_0\mathbf{I} & 0 & \mathbf{I} & \dots & 0 & 0 & 0 & 0 & 0 & 0 \\ \vdots & \vdots & \vdots & \vdots & \vdots & \vdots & \ddots & \vdots & \vdots & \vdots & \vdots & \vdots & \vdots \\ 0 & 0 & 0 & 0 & 0 & 0 & \dots & \mathbf{L}_1 & \mathbf{L}_2 & \mathbf{L}_3 & \mathbf{Keff} & 0 & 0 \\ 0 & 0 & 0 & 0 & 0 & 0 & \dots & a_1\mathbf{I} & \mathbf{I} & 0 & -a_1\mathbf{I} & \mathbf{I} & 0 \\ 0 & 0 & 0 & 0 & 0 & 0 & \dots & a_0\mathbf{I} & a_2\mathbf{I} & \mathbf{I} & -a_0\mathbf{I} & 0 & \mathbf{I} \end{bmatrix}, \tag{12}$$

where:

$$\begin{aligned} a_0 = \frac{4}{(\Delta t)^2}, a_1 = \frac{2}{\Delta t}, a_2 = \frac{4}{\Delta t}, \\ \mathbf{Keff} = a_0\mathbf{M} + a_1\mathbf{C} + \mathbf{K}, \quad \mathbf{L}_1 = -a_0\mathbf{M} - a_1\mathbf{C}, \\ \mathbf{L}_2 = -a_2\mathbf{M} - \mathbf{C}, \quad \mathbf{L}_3 = -\mathbf{M}. \end{aligned} \tag{13}$$

4 INVERSE MODELING

Control parameters ξ—horizontal and vertical components of force vector $\hat{\mathbf{F}}^{\mathrm{inv}}$—are iteratively updated with the aim to minimize the misfit between the measured ground motions and the reconstructed counterparts on the ground surface sensor locations. The following discrete objective functional is used in the minimization:

$$\hat{\mathcal{L}} = \frac{1}{2}(\hat{\mathbf{d}} - \hat{\mathbf{d}}^{\mathrm{m}})^T \overline{\mathbf{B}} (\hat{\mathbf{d}} - \hat{\mathbf{d}}^{\mathrm{m}}), \tag{14}$$

where $\hat{\mathbf{d}}$ is obtained by a set of estimated ξ; $\hat{\mathbf{d}}^m$ is generated by external force localized in the enlarged domain; and $\overline{\mathbf{B}}$ is a block diagonal matrix defined as $\Delta t\mathbf{B}$, in which $\mathbf{B}$ is a square matrix that is zero

everywhere except on the diagonal components corresponding to sparsely-distributed sensors' nodal locations. Then, the Lagrangian functional $\hat{\mathcal{A}}$ is built as:

$$\hat{\mathcal{A}} = \frac{1}{2}(\hat{\mathbf{d}} - \hat{\mathbf{d}}^{\mathrm{m}})^T \overline{\mathbf{B}} (\hat{\mathbf{d}} - \hat{\mathbf{d}}^{\mathrm{m}}) - \hat{\lambda}^T (\mathbf{Q}\hat{\mathbf{d}} - \hat{\mathbf{F}}^{\mathrm{inv}}). \tag{15}$$

The following three optimality conditions must be satisfied in order to determine the targeted control parameters. The first condition results in the state problem:

$$\frac{\partial \hat{\mathcal{A}}}{\partial \hat{\lambda}} = -\mathbf{Q}\hat{\mathbf{d}} + \hat{\mathbf{F}}^{\mathrm{inv}} = 0. \tag{16}$$

The second condition results in the discrete adjoint problem:

$$\frac{\partial \hat{\mathcal{A}}}{\partial \hat{\mathbf{d}}} = \underbrace{-\mathbf{Q}^T \hat{\lambda} + \overline{\mathbf{B}} (\hat{\mathbf{d}} - \hat{\mathbf{d}}^{\mathrm{m}}) = 0}_{\text{adjoint problem}}. \tag{17}$$

The adjoint problem is solved by marching backward over time. In our previous work [10], we showed a solution method to Eq. (17). Then, the third condition leads to the control equation:

$$\frac{\partial \hat{\mathcal{A}}}{\partial \hat{\mathbf{F}}^{\mathrm{inv}}} = \hat{\lambda} = 0. \tag{18}$$

Finally, by following the findings from our previous work [9], we use modified free-field waves in the DRM theory, leading to a modified reference effective seismic force $\hat{\mathbf{F}}^{\mathrm{ref}}_{\mathrm{mod}}$ as an alternative reference force. Then, the inverted effective force $\hat{\mathbf{F}}^{\mathrm{inv}}$ is post-processed to $\hat{\mathbf{F}}^{\mathrm{inv}}_{\mathrm{pp}}$, providing a direct comparison with $\hat{\mathbf{F}}^{\mathrm{ref}}_{\mathrm{mod}}$.

5 NUMERICAL EXPERIMENTS

In this numerical experiment we investigate the performance of the outlined inversion approach for identifying an effective seismic force at a DRM layer from seismic data and reconstructing the ground motions—induced by surface wave-dominant incident waves from an enlarged domain—in a interior domain Ω_i.

The extent of the enlarged domain is set to be 80 m by 40 m, surrounded by a 10 m-thick PML buffer at the left, bottom, and right sides (see Fig. 1). The shear wave speeds are V_{s_1}= 200 m/s, V_{s_2}= 150 m/s, V_{s_3}= 100 m/s, V_{s_4}= 500 m/s, and V_{s_5}= 800 m/s; the dilatational wave speeds are V_{p_1}= 400 m/s, V_{p_2}= 300 m/s, V_{p_3}= 200 m/s, V_{p_4}= 1000 m/s, and V_{p_5}= 1600 m/s; and the mass density of the entire domain is 1500 kg/m³. The solid on the top surface mimics a superstructure and its shear and dilatational wave speeds are V_{s_6} = 3250 m/s and V_{p_6} = 5900 m/s, respectively, being much larger than those in the layers under the superstructure. The targeted ground motions are induced by surface wave-dominant waves of central frequency of 5 Hz, characterized by a Ricker wavelet signal. Moreover, 19 sensors distributed on the top surface (i.e., sensor spacing of 2 m) are used in this example.

The DRM domain truncated by CFS-PML, shown in Fig. 2, is used in the inversion procedure. Its extent is 40 m by 20 m, surrounded by a 10 m-thick PML buffer. By the DRM theory, the modified reference effective force $\hat{\mathbf{F}}^{\mathrm{ref}}_{\mathrm{mod}}$ and the post-processed inverted effective force $\hat{\mathbf{F}}^{\mathrm{inv}}_{\mathrm{pp}}$ are applied on all the nodes of the virtual interface boundaries Γ_b, Γ_m, and Γ_e (i.e., the dashed lines in Fig. 2).

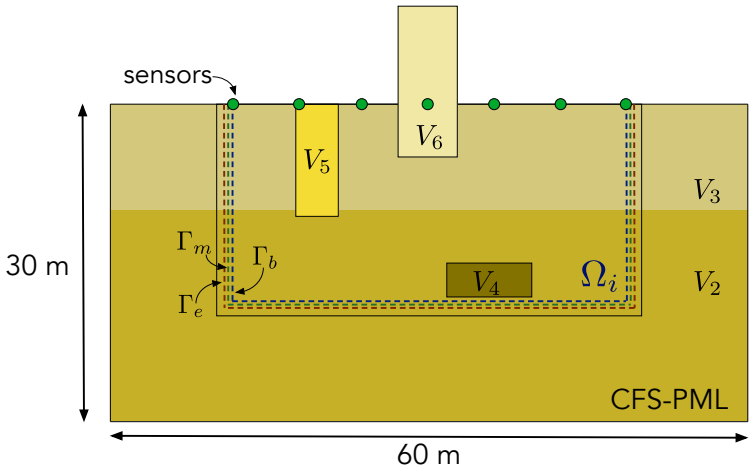

Figure 2: Inversion solver configuration: a DRM domain truncated by CFS-PML.

For appraising the accuracy of the presented method, the error norms $\mathcal{E}^{|u|}$, $\mathcal{E}^{u_x}$, and $\mathcal{E}^{u_y}$ are calculated to evaluate the inversion performance to reconstruct the amplitude of ground motions, horizontal displacements, and vertical displacements in Ω_i.

Fig. 3 shows the targeted and reconstructed ground motions' displacement amplitudes in Ω_i for three different timesteps. After 500 iterations, the error $\mathcal{E}^{|u|}$ between the amplitude of targeted wave responses and their estimated counterparts is only 0.34%. Figs. 4 and 5 show the targeted horizontal and vertical displacements and their reconstructed counterparts, respectively. The error $\mathcal{E}^{u_x}$ and $\mathcal{E}^{u_y}$ are 1.20% and 0.39%, respectively. Thus, the presented inversion solver can effectively estimate the wave responses, induced by surface wave-dominant incident waves, in a reduced domain, Ω_i, and superstructure.

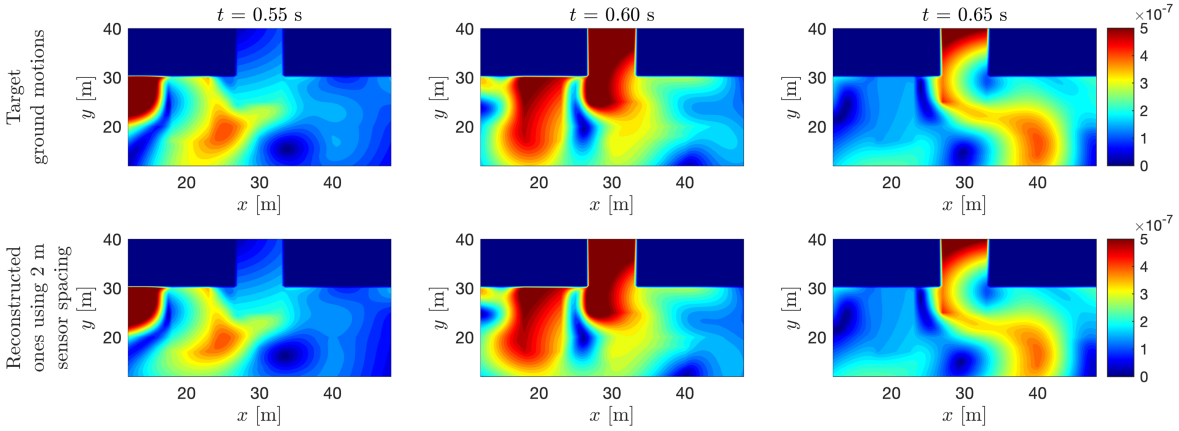

Figure 3: (Upper figures) Targeted ground motions' displacement amplitude ($|u|$) in Ω_i induced by surface wave-dominant incident waves and (Lower figures) their reconstructed counterparts.

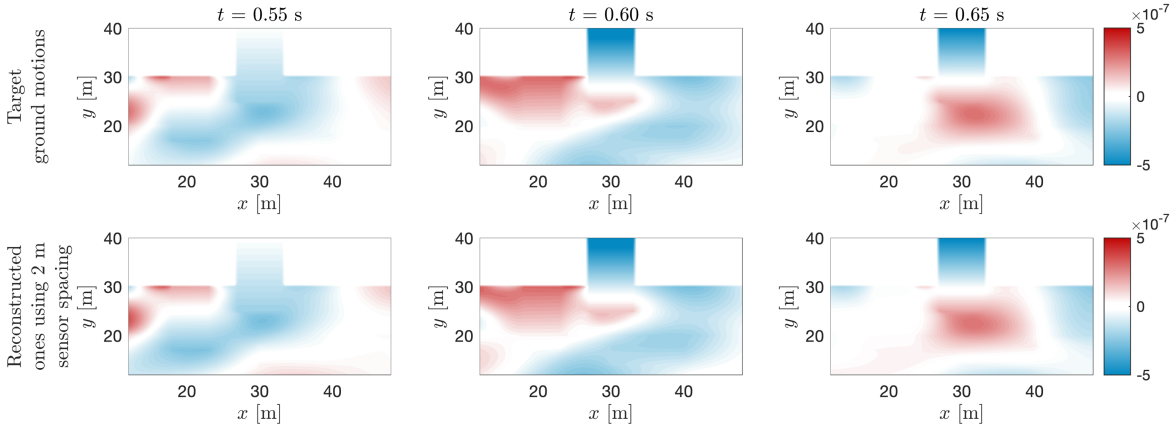

Figure 4: (Upper figures) Targeted horizontal displacements (u_x) of wave motions in Ω_i induced by surface wave-dominant incident waves and (Lower figures) their reconstructed counterparts.

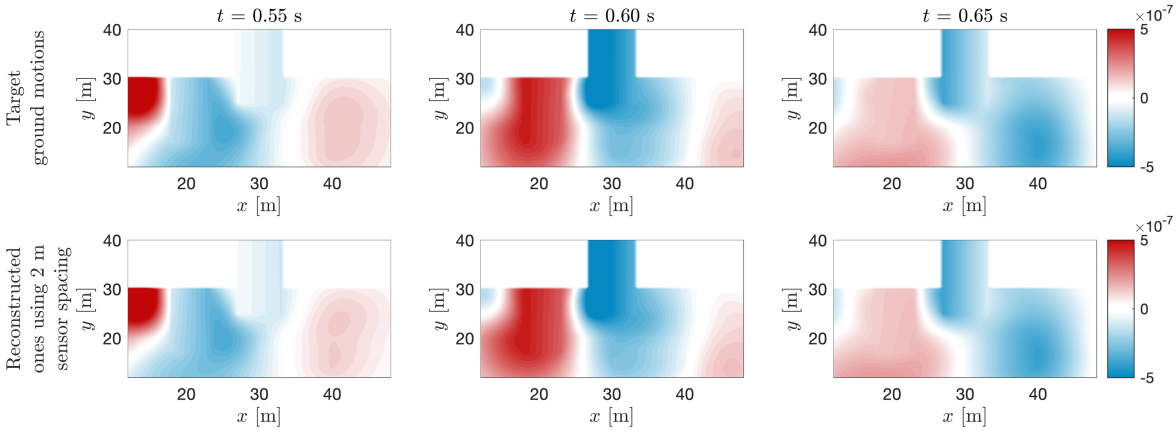

Figure 5: (Upper figures) Targeted vertical displacements (u_y) of wave motions in Ω_i induced by surface wave-dominant incident waves and (Lower figures) their reconstructed counterparts.

Fig. 6, 7, and 8 show that the horizontal and vertical components of modified reference effective force $\hat{\mathbf{F}}^{\text{ref}}_{\text{mod}}$ are in excellent agreement with those of post-processed inverted effective force $\hat{\mathbf{F}}^{\text{inv}}_{\text{pp}}$ on Γ_b, Γ_m, and Γ_e, respectively. Namely, the error norm $\mathcal{E}$ between all components of $\hat{\mathbf{F}}^{\text{ref}}_{\text{mod}}$ and those of $\hat{\mathbf{F}}^{\text{inv}}_{\text{pp}}$ is 4.60%. The error $\mathcal{E}_x$, which considers only the horizontal components of $\hat{\mathbf{F}}^{\text{ref}}_{\text{mod}}$ and $\hat{\mathbf{F}}^{\text{inv}}_{\text{pp}}$, and the error $\mathcal{E}_y$, which considers only the vertical components, are 26.01% and 1.89%, respectively. Thus, the presented inversion solver can identify an effective seismic force (equivalent to an incident wave) at a DRM layer from seismic data.

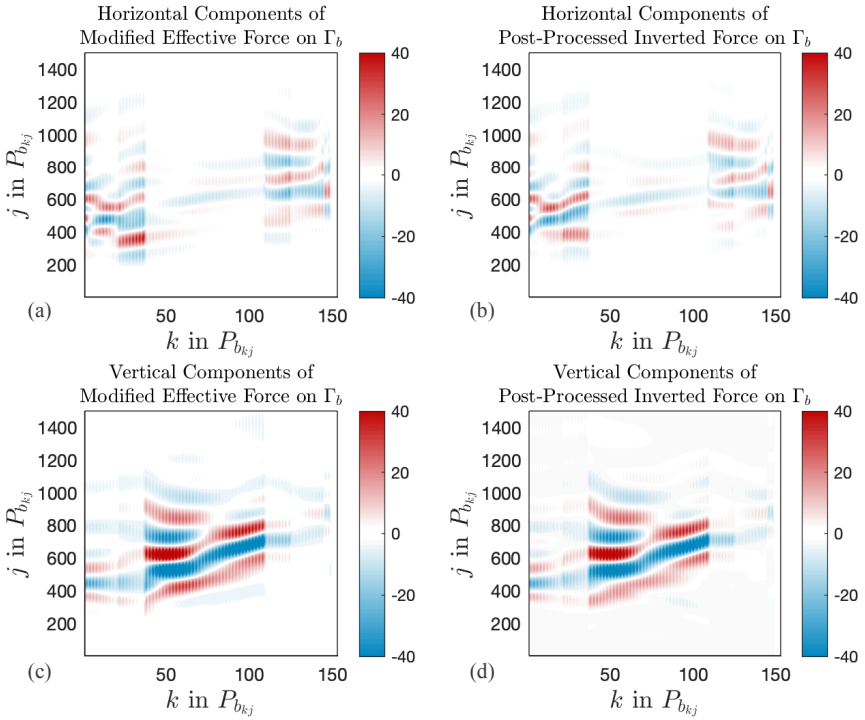

Figure 6: Horizontal (a,b) and vertical (c,d) components of modified reference effective seismic force and their post-processed inverted counterparts on Γ_b.

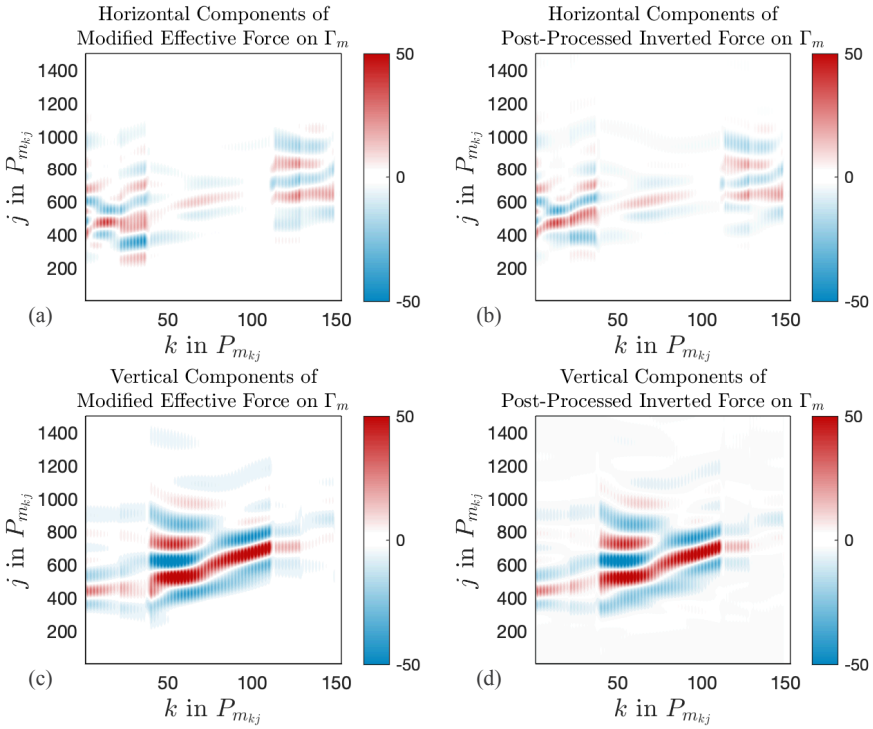

Figure 7: Horizontal (a,b) and vertical (c,d) components of modified reference effective seismic force and their post-processed inverted counterparts on Γ_m.

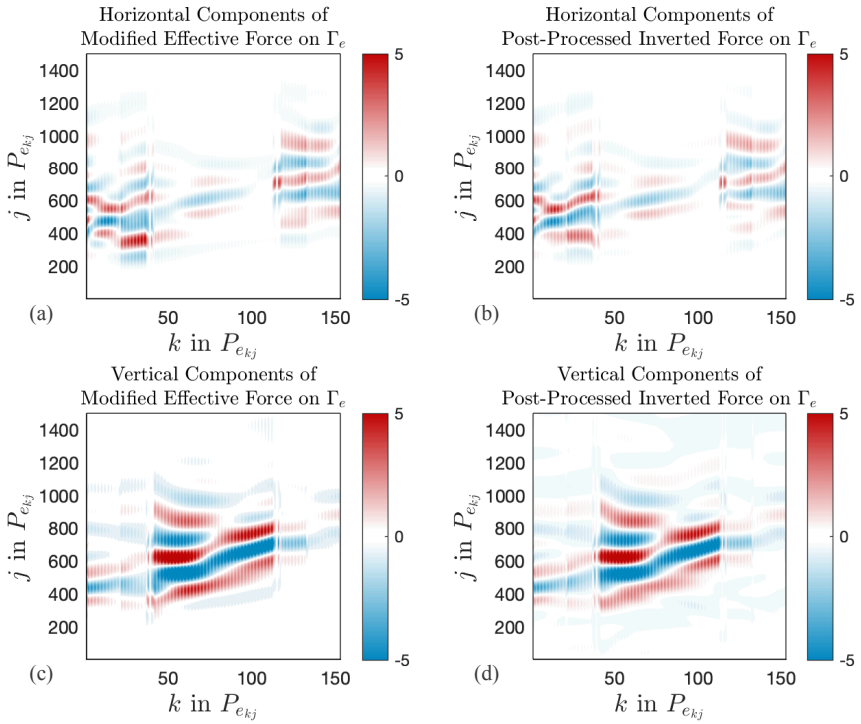

Figure 8: Horizontal (a,b) and vertical (c,d) components of modified reference effective seismic force and their post-processed inverted counterparts on Γ_e.

6 CONCLUSIONS

We introduced a novel inverse modeling method for estimating ground movements in a 2D interior domain surrounded by the DRM layer and truncated by CFS-PML. The minimization problem searches nodal forces at the DRM layer to minimize a misfit between measured ground motions at sparsely-distributed sensors and their reconstructed counterparts. In the presented method, the sensors are placed only on the top surface of the domain. The presented full-waveform inversion method can reconstruct the ground motions in a reduced domain and those in a superstructure. Moreover, the presented inversion solver can identify an effective seismic force at a DRM layer, which is equivalent to an incident wave. Extending the discussed inversion method to 3D settings can help geotechnical earthquake engineers so that they may model the influence of an earthquake on near-surface environments. Then, the information on possible risk areas can be shared and help decision-makers quickly plan the budget and schedule repairs after an earthquake event.

7 ACKNOWLEDGMENTS

This material is based upon work supported by the National Science Foundation (NSF) under Award No. CMMI-2044887 and 2053694. Any opinions, findings, and conclusions or recommendations expressed in this material are those of the authors and do not necessarily reflect the views of the NSF. The authors are also grateful for the support by the Faculty Research and Creative Endeavors (FRCE) Research Grant-48058 at Central Michigan University.

References

[1] AKCELIK, V., BIROS, G., AND GHATTAS, O. Parallel multiscale Gauss-Newton-Krylov methods for inverse wave propagation. In *Supercomputing, ACM/IEEE 2002 Conference* (2002), IEEE, pp. 41–41.

[2] ASKAN, A., AKCELIK, V., BIELAK, J., AND GHATTAS, O. Full Waveform Inversion for Seismic Velocity and Anelastic Losses in Heterogeneous Structures. *Bulletin of the Seismological Society of America 97*, 6 (12 2007), 1990–2008.

[3] ASKAN, A., AKCELIK, V., BIELAK, J., AND GHATTAS, O. Parameter sensitivity analysis of a nonlinear least-squares optimization-based anelastic full waveform inversion method. *Comptes Rendus Mécanique 338*, 7 (2010), 364 – 376. Inverse problems.

[4] ASKAN, A., AND BIELAK, J. Full Anelastic Waveform Tomography Including Model Uncertainty. *Bulletin of the Seismological Society of America 98*, 6 (12 2008), 2975–2989.

[5] BIELAK, J., LOUKAKIS, K., HISADA, Y., AND YOSHIMURA, C. Domain reduction method for three-dimensional earthquake modeling in localized regions, Part I: Theory. *Bulletin of the Seismological Society of America 93*, 2 (2003), 817–824.

[6] FATHI, A., KALLIVOKAS, L. F., AND POURSARTIP, B. Full-waveform inversion in three-dimensional PML-truncated elastic media. *Computer Methods in Applied Mechanics and Engineering 296* (2015), 39–72.

[7] FATHI, A., POURSARTIP, B., STOKOE II, K. H., AND KALLIVOKAS, L. F. Three-dimensional P-and S-wave velocity profiling of geotechnical sites using full-waveform inversion driven by field data. *Soil Dynamics and Earthquake Engineering 87* (2016), 63–81.

[8] FRANÇOIS, S., GOH, H., AND KALLIVOKAS, L. F. Non-convolutional second-order complex-frequency-shifted perfectly matched layers for transient elastic wave propagation. *Computer Methods in Applied Mechanics and Engineering 377* (2021), 113704.

[9] GUIDIO, B., HEEDONG, G., AND JEONG, C. Effective seismic force retrieval from surface measurement for SH-wave reconstruction (under review), 2022.

[10] GUIDIO, B., JEREMIĆ, B., GUIDIO, L., AND JEONG, C. Passive seismic inversion of sh wave input motions in a truncated domain. *Soil Dynamics and Earthquake Engineering 158* (2022), 107263.

[11] GUIDIO, B. P., AND JEONG, C. Full-waveform inversion of incoherent dynamic traction in a bounded 2D domain of scalar wave motions. *Journal of Engineering Mechanics 147*, 4 (2021), 04021010.

[12] JEONG, C., NA, S.-W., AND KALLIVOKAS, L. F. Near-surface localization and shape identification of a scatterer embedded in a halfplane using scalar waves. *Journal of Computational Acoustics 17*, 03 (2009), 277–308.

[13] JEONG, C., AND SEYLABI, E. E. Seismic input motion identification in a heterogeneous halfspace. *Journal of Engineering Mechanics 144*, 8 (2018), 04018070.

[14] JU, S. H. A Deconvolution scheme for determination of seismic loads in finite element analyses. *Bulletin of the Seismological Society of America 103*, 1 (Feb. 2013), 258–267.

[15] KANG, J. W., AND KALLIVOKAS, L. F. The inverse medium problem in 1D PML-truncated heterogeneous semi-infinite domains. *Inverse Problems in Science and Engineering 18*, 6 (2010), 759–786.

[16] MEJIA, L., AND DAWSON, E. Earthquake deconvolution for FLAC. *FLAC and Numerical* (2006).

[17] PAKRAVAN, A., KANG, J. W., AND NEWTSON, C. M. A Gauss-Newton full-waveform inversion for material profile reconstruction in viscoelastic semi-infinite solid media. *Inverse Problems in Science and Engineering 24*, 3 (Mar. 2016), 393–421.

[18] POUL, M. K., AND ZERVA, A. Efficient time-domain deconvolution of seismic ground motions using the equivalent-linear method for soil-structure interaction analyses. *Soil Dynamics and Earthquake Engineering 112* (2018), 138 – 151.

[19] POUL, M. K., AND ZERVA, A. Nonlinear dynamic response of concrete gravity dams considering the deconvolution process. *Soil Dynamics and Earthquake Engineering 109* (2018), 324 – 338.

[20] TRAN, K. T., AND MCVAY, M. Site characterization using Gauss-Newton inversion of 2-D full seismic waveform in the time domain. *Soil Dynamics and Earthquake Engineering 43* (Dec. 2012), 16–24.

[21] YOSHIMURA, C., BIELAK, J., HISADA, Y., AND FERNÁNDEZ, A. Domain reduction method for three-dimensional earthquake modeling in localized regions, part II: Verification and applications. *Bulletin of the Seismological Society of America 93*, 2 (2003), 825–841.